ELSEVIER

Composites: Part B 33 (2002) 25–34

composites
Part B: engineering

www.elsevier.com/locate/compositesb

A damage mechanics model of crack-weakened, chopped fiber composites under impact loading ☆

H.K. Lee[a,*], S. Simunovic[b]

[a]Department of Civil, Architectural, and Environmental Engineering, University of Miami, Coral Gables, FL 33124-0620, USA
[b]Computer Science and Mathematics Division, Oak Ridge National Laboratory, Oak Ridge, TN 37831-6359, USA

Received 28 November 2000; accepted 3 September 2001

Abstract

A micromechanical approach recently proposed by Lee and Simunovic [Compos. Part B: Engng. 31 (2000) 77] is introduced to develop analytical and numerical models that efficiently predict the behavior of chopped fiber based composites containing microcracks under impact loading. Based on the ensemble-volume averaging process and the first-order effects of eigenstrains due to the existence of chopped fibers and microcracks, an effective yield criterion of the composites is derived. Microcracks in the matrix are considered by employing the Eshelby's equivalence principle and their influence on the stress–strain relations of the composites is investigated. Further, the Weibull's probabilistic function is used to model the varying probability of progressive partial fiber debonding. The developed micromechanical constitutive model is then implemented into the finite element code DYNA3D to perform impact simulation of the composites. Finally, numerical simulations for cantilever beam test and composite contact test are carried out to validate the finite element implementation and predict the impact behavior of composite structures. © 2002 Published by Elsevier Science Ltd.

Keywords: C. Damage mechanics; C. Finite element analysis (FEA); B. Impact behavior; Crack-weakened composites

1. Introduction

The goal of automotive engineers today is to provide lightweight, more fuel-efficient automobiles capable of greater crashworthiness. In the crashworthiness of automotive structures, the primary issues are the overall economy and the weight of the material. To reduce the weight and improve the fuel economy, fiber-reinforced polymer composites have replaced more and more metal parts in vehicles. Carbon fiber composites, which are new breed of high-strength materials, have attracted worldwide attention and hold great promise due to their attributes of high strength-to-weight and stiffness-to-weight ratios, corrosion resistance and fatigue resistance. In comparison to metals, carbon fibers are generally characterized by a brittle rather than ductile response to the applied loads, especially in compression. Thus, they are used in composites with a lightweight matrix. Recently, the automotive industry has been interested in investigating the use of carbon and glass fibers in chopped fiber-reinforced composites that are generally considered to have the potential to satisfy today's requirements as well as or better than other materials.

The major difference, however, is that metal structures collapse under crush or impact by buckling and/or folding in accordion type fashion involving extensive plastic deformation, whereas chopped fiber composites fail through a sequence of fracture mechanisms. The actual mechanisms (e.g. matrix cracking, fiber–matrix debonding, and sequence of damage) are highly dependent on fiber length, tow size, crush speed, triggers and geometry of the structure. Experimental investigations of fiber-reinforced tubes and cones indicate a wide range of material damage such as matrix crushing, fiber–matrix debonding, and fiber breakage. The first two types of failure often show a rather slowly progressing failure with high-energy dissipation, while the last failure type might initiate a catastrophic collapse of the entire structure with little dissipation of kinetic energy. It is noted that the microscopic failure behavior of the composites is still not completely understood. Nevertheless, several attempts towards the simulation of a composite crash have been made [2–4]. A more detailed review of failure in fiber-reinforced composites can be seen in studies

☆ The submitted manuscript has been authored by a contractor of the US Government under contract No. DE-AC05-96OR22464. Accordingly, the US Government retains a nonexclusive, royalty-free license to publish or reproduce the published form of this contribution, or allow others to do so, for US Government purposes.

* Corresponding author. Tel.: +1-305-284-3457; fax: +1-305-284-3492.
E-mail address: hlee@miami.edu (H.K. Lee).

1359-8368/02/$ - see front matter © 2002 Published by Elsevier Science Ltd.
PII: S1359-8368(01)00048-8

by Matzenmiller and Schweizerhof [2], Kutlu and Chang [5], and Meraghni and Benzeggagh [6].

While there is substantial research in the aerospace community on graphite–fiber laminated composites, there is very little information pertaining to the response of carbon fiber composites during automotive impact-induced crash loading conditions. Currently, the predictive analytical and numerical tools required to accurately evaluate and design carbon fiber automotive structures for crush do not exist. In order to successfully develop these predictive tools, a micromechanical damage constitutive model for chopped fiber-reinforced composites is developed. This work focuses specifically on development of analytical and numerical models that efficiently predict the behavior of chopped fiber based composites in vehicular impact simulations.

In our derivation, chopped fibers are assumed to be elastic (prolate) spheroids that are randomly oriented in a ductile polymer matrix. Penny-shaped microcracks are regarded as the limiting case of oblate spheroidal voids and are assumed to retain the uniform size and the same volume fraction during the deformations. However, it is possible to extend the proposed model to accommodate cracks with different size and orientation in the matrix by adding the corresponding inclusion phases. The Weibull's probabilistic function is used to model the varying probability of progressive partial fiber debonding. It is also assumed that after the interfacial debonding between the fibers and the matrix, these partially debonded fibers are replaced by equivalent, transversely isotropic inclusions. Only dilute or moderate fiber reinforced composites will be considered here.

The damage constitutive model is then implemented into the open source finite element code DYNA3D to perform the impact simulation of the composites. Finally, numerical simulations for cantilever beam test and composite contact test are carried out to validate the finite element implementation and compare with experimental data.

2. Overall elastoplastic behavior of crack-weakened, chopped fiber composites

2.1. Effective elastic moduli of crack-weakened, chopped fiber composites

First, an initially perfectly bonded, three-phase composite consisting of a matrix (phase 0) with bulk modulus κ_0 and shear modulus μ_0; aligned discontinuous, randomly dispersed, (prolate) spheroidal fibers (phase 1) with bulk modulus κ_1 and shear modulus μ_1; and aligned penny-shaped microcracks (phase 2) is considered. When spheroidal inclusions (discontinuous fibers and penny-shaped microcracks) are aligned, the composite as a whole is transversely isotropic. Subsequently, as loadings or deformations are applied, some fibers are partially debonded (phase 3). These partially debonded fibers are regarded as equivalent, transversely isotropic inclusions. Following Zhao and Weng [7,8] and Ju and Lee [9], a partially debonded fiber can be replaced by an equivalent, perfectly bonded fiber that possesses yet unknown transversely isotropic moduli. Penny-shaped microcracks are assumed to remain the uniform size and the same microcrack density during the deformations.

Based on Ju and Chen's [10] governing field equations for linear elastic composites containing arbitrarily nonaligned and/or dissimilar ellipsoidal inclusions, the effective elastic stiffness tensor $\mathbf{C}_*$ for aligned, crack-weakened, chopped fiber composites were derived by Lee [11] as

$$\mathbf{C}_* = \tilde{F}_{ijkl}(\tau_1, \tau_2, \tau_3, \tau_4, \tau_5, \tau_6) \tag{1}$$

where the definition of fourth-rank tensor $\tilde{\mathbf{F}}$ is given in Eq. (2) of Lee and Simunovic [1] and the inverse and product of a fourth-rank tensor $\tilde{\mathbf{F}}$ are given in the appendix of Ju and Chen [12]. The components $\tau_1, \ldots, \tau_6$ are also given in the appendix of Lee [11].

Assuming all fibers and microcracks in the composite changed from aligned array to three-dimensional random array, the effective elastic moduli of (randomly oriented) chopped fiber composites can be obtained by applying the orientational averaging process proposed by Lee and Simunovic [1]. Assuming the uniform distribution of overall strains, the effective elastic stiffness tensor $\subset \mathbf{C}_* \supset$ in Eq. (1) is averaged over all orientations as

$$\begin{aligned} \subset \mathbf{C}_* \supset &= \frac{1}{2\pi} \int_0^{\pi} \int_0^{\pi} l_{mi} l_{nj} (C_*)_{mnpq} l_{pk} l_{ql} \sin\theta \, \mathrm{d}\theta \, \mathrm{d}\phi \\ &= \mathscr{C}_1 \delta_{ij} \delta_{kl} + \mathscr{C}_2 (\delta_{ik} \delta_{jl} + \delta_{il} \delta_{jk}) \end{aligned} \tag{2}$$

with

$$\mathscr{C}_1 = \frac{1}{15}[\tau_1 + 5(\tau_3 + \tau_4 + 3\tau_5)] \tag{3}$$

$$\mathscr{C}_2 = \frac{1}{15}[\tau_1 + 10\tau_2 + 15\tau_6] \tag{4}$$

where l_{ij} signifies the directional cosine between ith primed and jth unprimed axes.

2.2. Effective elastoplastic behavior of crack-weakened, chopped fiber composites

Let us consider the overall elastoplastic responses of aligned, crack-weakened, chopped fiber composites that initially feature perfect interfacial bonding between fibers and the matrix in three-phase composites. For simplicity, the von Mises yield criterion with isotropic hardening law is assumed here.

Following Lee and Simunovic [13], we denote the square of the 'current stress norm' by $H(\mathbf{x}|\mathscr{G}\})$ at the local point $\mathbf{x}$, which determines the plastic strain in a composite for a given phase configuration $\mathscr{G}$. Since there is no plastic strain in the elastic perfectly bonded fibers, partially debonded fibers, or penny-shaped microcracks, $H(\mathbf{x}|\mathscr{G})$ can

be written as

$$H(\mathbf{x}|\mathscr{G}) = \begin{cases} \boldsymbol{\sigma}(\mathbf{x}|\mathscr{G}) : \mathbf{I}_{\mathrm{d}} : \boldsymbol{\sigma}(\mathbf{x}|\mathscr{G}), & \text{if } \mathbf{x} \text{ in the matrix;} \\ 0, & \text{otherwise.} \end{cases} \tag{5}$$

where $\mathbf{I}_{\mathrm{d}}$ signifies the deviatoric part of the fourth-rank identity tensor $\mathbf{I}$.

In addition, $\langle H\rangle_{\mathrm{m}}(\mathbf{x})$ is defined as the ensemble average of $H(\mathbf{x}|\mathscr{G})$ over all possible realizations where $\mathbf{x}$ is in the matrix phase. Here, the angled bracket $\langle\cdot\rangle$ signifies the ensemble average operator. Let $P(\mathscr{G}_q)$ be the probability density function for finding the q-phase ($q = 1, 2, 3$) configuration $\mathscr{G}_q$ in the composite. $\langle H\rangle_{\mathrm{m}}(\mathbf{x})$ can be obtained by integrating H over all possible perfectly bonded fibers, partially debonded fibers, and penny-shaped microcracks configurations (for a point $\mathbf{x}$ in the matrix)

$$\begin{aligned} \langle H\rangle_{\mathrm{m}}(\mathbf{x}) = H^{\mathrm{o}} &+ \int_{\mathscr{G}_1} \{H(\mathbf{x}|\mathscr{G}_1) - H^{\mathrm{o}}\} P(\mathscr{G}_1)\, \mathrm{d}\mathscr{G} \\ &+ \int_{\mathscr{G}_2} \{H(\mathbf{x}|\mathscr{G}_2) - H^{\mathrm{o}}\} P(\mathscr{G}_2)\, \mathrm{d}\mathscr{G} \\ &+ \int_{\mathscr{G}_3} \{H(\mathbf{x}|\mathscr{G}_2) - H^{\mathrm{o}}\} P(\mathscr{G}_3)\, \mathrm{d}\mathscr{G} \end{aligned} \tag{6}$$

where H^{o} is the square of the far-field stress norm in the matrix:

$$H^{\mathrm{o}} = \boldsymbol{\sigma}^{\mathrm{o}} : \mathbf{I}_{\mathrm{d}} : \boldsymbol{\sigma}^{\mathrm{o}} \tag{7}$$

in which $\boldsymbol{\sigma}^{\mathrm{o}}$ denotes the far-field stress.

As indicated, a matrix point receives the perturbations from perfectly bonded fibers, partially debonded fibers, and penny-shaped microcracks. Therefore, the ensemble-average stress norm for any matrix point $\mathbf{x}$ can be evaluated by collecting and summing up all the current stress norm perturbations produced by any typical perfectly bonded fiber centered at $\mathbf{x}_1^{(1)}$ in the perfectly bonded fiber domain; any typical penny-shaped microcrack centered at $\mathbf{x}_2^{(1)}$ in the penny-shaped microcrack domain; and any typical partially debonded fiber centered at $\mathbf{x}_3^{(1)}$ in the partially debonded fiber domain; and averaging over all possible locations of $\mathbf{x}_1^{(1)}$, $\mathbf{x}_2^{(1)}$, and $\mathbf{x}_3^{(1)}$. As a result, we arrive at

$$\begin{aligned} \langle H\rangle_{\mathrm{m}}(\mathbf{x}) \cong H^{\mathrm{o}} &+ \int_{\mathbf{x}_1^{(1)} \notin \Xi(\mathbf{x})} \left\{H\left(\mathbf{x}|\mathbf{x}_1^{(1)}\right) - H^{\mathrm{o}}\right\} P\left(\mathbf{x}_1^{(1)}\right) \mathrm{d}\mathbf{x}_1^{(1)} \\ &+ \int_{\mathbf{x}_2^{(1)} \notin \Xi(\mathbf{x})} \left\{H\left(\mathrm{x}|\mathrm{x}_2^{(1)}\right) - H^{\mathrm{o}}\right\} P\left(\mathrm{x}_2^{(1)}\right) \mathrm{d}\mathbf{x}_2^{(1)} \\ &+ \int_{\mathbf{x}_3^{(1)} \notin \Xi(\mathbf{x})} \left\{H\left(\mathbf{x}|\mathbf{x}_3^{(1)}\right) - H^{\mathrm{o}}\right\} P\left(\mathbf{x}_3^{(1)}\right) \mathrm{d}\mathbf{x}_3^{(1)} \\ &+ \ldots \end{aligned} \tag{8}$$

where $\Xi(\mathbf{x})$ is the exclusion zone and $P(\mathbf{x}_1^{(1)})$, $P(\mathbf{x}_2^{(1)})$, and $P(\mathbf{x}_3^{(1)})$ denote the probability density functions for finding a perfectly bonded fiber centered at $\mathbf{x}_1^{(1)}$, a penny-shaped microcrack centered at $\mathbf{x}_2^{(1)}$, and a partially debonded fiber centered at $\mathbf{x}_3^{(1)}$, respectively. Here, $P(\mathbf{x}_1^{(1)})$, $P(\mathbf{x}_2^{(1)})$, and $P(\mathbf{x}_3^{(1)})$ are assumed to be statistically homogeneous, isotropic, and uniform for simplicity. That is, we assume that the probability density functions take the form $P(\mathbf{x}_1^{(1)}) = N_1/V$, $P(\mathbf{x}_2^{(1)}) = N_2/V$ and $P(\mathbf{x}_3^{(1)}) = N_3/V$, where N_1, N_2, and N_3 are the total numbers of perfectly bonded fibers, penny-shaped microcracks, and partially debonded fibers, respectively, dispersed in a representative volume V. Accordingly, the volume fraction of the rth phase inclusion can be defined as $\phi_r = (4\pi/3)(N_r/V)a_2^3$.

By dropping higher order terms, the integral on the right-hand side of Eq. (8) can be evaluated and we arrive at the ensemble-averaged current stress norm at any matrix point:

$$\langle H\rangle_{\mathrm{m}}(\mathbf{x}) = \boldsymbol{\sigma}^{\mathrm{o}} : \mathbf{T} : \boldsymbol{\sigma}^{\mathrm{o}} \tag{9}$$

The components of the positive definite fourth-rank tensor $\mathbf{T}$ read

$$T_{ijkl} = \tilde{F}_{ijkl}(\eta_1, \eta_2, \eta_3, \eta_4, \eta_5, \eta_6) \tag{10}$$

where the six parameters on the right-hand side take the form

$$\begin{aligned} \eta_1 &= \Phi_{11} - \Phi_{12} - \Phi_{21} + \Phi_{22} + 2\Psi_1 + 2\Psi_2 - 4\Psi_3 \\ \eta_2 &= -\Psi_2 + \Psi_3 \\ \eta_3 &= \Phi_{21} - \Phi_{23} \\ \eta_4 &= \Phi_{12} - \Phi_{23} \\ \eta_5 &= \Phi_{23} \\ \eta_6 &= \Psi_2 \end{aligned} \tag{11}$$

in which the parameters Φ_{ij} and Φ_i are given in Appendix A.

We now consider the overall elastoplastic responses of crack-weakened, (randomly oriented) chopped fiber composites in three-dimensional space. By applying the orientational averaging process to Eq. (9), the orientation-averaged square of stress norm $\subset H_{\mathrm{m}} \supset$ at any matrix point can be obtained as

$$\subset H_{\mathrm{m}} \supset = \boldsymbol{\sigma}^{\mathrm{o}} :\subset \mathbf{T} \supset: \boldsymbol{\sigma}^{\mathrm{o}} \tag{12}$$

where the isotropic fourth-rank tensor $\subset \mathbf{T} \supset$ is

$$\subset T_{ijkl} \supset = \frac{1}{2\pi} \int_0^{\pi} \int_0^{\pi} l_{mi} l_{nj} T_{mnpq} l_{pk} l_{ql} \sin\theta \, \mathrm{d}\theta \, \mathrm{d}\phi \tag{13}$$

The components of the positive definite fourth-rank tensor $\subset \mathbf{T} \supset$ read

$$\subset T_{ijkl} \supset = \bar{\eta}_1 \delta_{ij}\delta_{kl} + \bar{\eta}_2(\delta_{ik}\delta_{jl} + \delta_{il}\delta_{jk}) \tag{14}$$

with

$$\bar{\eta}_1 = \frac{1}{15}[\eta_1 + 5(\eta_3 + \eta_4 + 3\eta_5)] \tag{15}$$

$$\bar{\eta}_2 = \frac{1}{15}[\eta_1 + 10\eta_2 + 15\eta_6] \tag{16}$$

where the parameters $\eta_1, \ldots, \eta_6$ are given in Eq. (11).

The ensemble-averaged current stress norm at a matrix point can also be expressed in terms of the macroscopic stress $\bar{\boldsymbol{\sigma}}$. Following Ju and Chen [10], the relation between the far-field stress $\boldsymbol{\sigma}^{\mathrm{o}}$ and the macroscopic stress $\bar{\boldsymbol{\sigma}}$ takes the form

$$\boldsymbol{\sigma}^{\mathrm{o}} = \mathbf{P} : \bar{\boldsymbol{\sigma}} \tag{17}$$

where the fourth-rank tensor $\mathbf{P}$ reads

$$\mathbf{P} = \left[\mathbf{I} + \sum_{r=1}^{3} \phi_r(\mathbf{I} - \mathbf{S}_r)\cdot(\mathbf{A}_r + \mathbf{S}_r)^{-1}\right]^{-1}$$

$$= \tilde{F}_{ijkl}(q_1, q_2, q_3, q_4, q_5, q_6) \tag{18}$$

and the components $q_1, \ldots, q_6$ are

$$q_1 = \mathscr{H}_{11} - \mathscr{H}_{12} - \mathscr{H}_{21} + \mathscr{H}_{22} + 2\mathscr{I}_1 + 2\mathscr{I}_2 - 4\mathscr{I}_3$$

$$q_2 = -\mathscr{I}_2 + \mathscr{I}_3$$

$$q_3 = \mathscr{H}_{21} = \mathscr{H}_{23}$$

$$q_4 = \mathscr{H}_{12} - \mathscr{H}_{23}$$

$$q_5 = \mathscr{H}_{23}$$

$$q_6 = \mathscr{I}_2 \tag{19}$$

with

$$\mathscr{H}_{ij} = -\frac{\mathscr{I}_{ij}}{2\mathscr{K}_i} \quad (i,j = 1,2,3) \tag{20}$$

$$\mathscr{I}_i = \frac{1}{4\mathscr{K}_i} \quad (i = 1,2,3) \tag{21}$$

where

$$\mathscr{I}_{i1} = \frac{(\mathscr{L}_{22} + \mathscr{K}_2)\mathscr{L}_{i1} - \mathscr{L}_{21}\mathscr{L}_{i2}}{(\mathscr{L}_{11} + 2\mathscr{K}_1)(\mathscr{L}_{22} + \mathscr{K}_2) - \mathscr{L}_{12}\mathscr{L}_{21}}$$

$$(i = 1,2,3) \tag{22}$$

$$\mathscr{I}_{i2} = \mathscr{I}_{i3} = \frac{(\mathscr{L}_{11} + 2\mathscr{K}_1)\mathscr{L}_{i2} - \mathscr{L}_{12}\mathscr{L}_{i1}}{2(\mathscr{L}_{11}2\mathscr{K}_1)(\mathscr{L}_{22} + \mathscr{K}_2) - 2\mathscr{L}_{12}\mathscr{L}_{21}}$$

$$(i = 1,2,3) \tag{23}$$

$$\mathscr{K}_i = \frac{1}{2} + \sum_{r=1}^{3} \frac{[1 - 2(\mathscr{B}_r)_i]\phi_r}{2(\mathscr{V}_r)_i}$$

$$(i = 1,2,3) \tag{24}$$

$$\mathscr{L}_{ij} = \sum_{r=1}^{3} \phi_r \sum_{n=1}^{3} \frac{(\mathscr{W}_r)_{nj}(\bar{\mathscr{A}}_r)_{in}}{(\mathscr{V}_r)_n} - \frac{(\bar{\mathscr{A}}_r)_{ij}}{(\mathscr{V}_r)_j} - \frac{(\mathscr{W}_r)_{ij}(1 - 2(\bar{\mathscr{B}}_r)_{ij}}{(\mathscr{V}_r)_i}$$

$$(i,j = 1,2,3) \tag{25}$$

in which the parameters $(\mathscr{B}_r)_i$, $(\mathscr{V}_r)_i$, $(\mathscr{W}_r)_{ij}$, $(\bar{\mathscr{A}}_r)_{ij}$, $(\bar{\mathscr{B}}_r)_{ij}$ are given in Appendix A.

By applying the orientational averaging process to Eq. (18), the orientation-averaged square of stress norm $\subset H_{\mathrm{m}} \supset$ at any matrix point can be obtained as

$$\boldsymbol{\sigma}^{\mathrm{o}} = \subset \mathbf{P} \supset : \subset \bar{\boldsymbol{\sigma}} \supset \tag{26}$$

where the fourth-rank tensor $\subset \mathbf{P} \supset$ reads

$$\subset P_{ijkl} \supset = \tilde{q}_1\delta_{ij}\delta_{kl} + \tilde{q}_2(\delta_{ik}\delta_{jl} + \delta_{il}\delta_{jk}) \tag{27}$$

with

$$\tilde{q}_1 = \frac{1}{15}[q_1 + 5(q_3 + q_4 + 3q_5)] \tag{28}$$

$$\tilde{q}_2 = \frac{1}{15}[q_1 + 10q_2 + 15q_6] \tag{29}$$

where the parameters $q_1, \ldots, q_6$ are given in Eq. (19).

By combining Eqs. (12) and (26), we arrive at the alternative expression for the orientation-averaged current stress norm (square) at a matrix point:

$$\subset H_{\mathrm{m}} \supset = \subset \bar{\boldsymbol{\sigma}} \supset : \subset \bar{\mathbf{T}} \supset : \subset \bar{\boldsymbol{\sigma}} \supset \tag{30}$$

where

$$\subset \bar{\mathbf{T}} \supset = \subset \mathbf{P} \supset^{\mathbf{T}} \cdot \subset \mathbf{T} \supset \cdot \subset \mathbf{P} \supset = \bar{T}_1\delta_{ij}\delta_{kl} + \bar{T}_2(\delta_{ik}\delta_{jl} + \delta_{il}\delta_{jk}) \tag{31}$$

with

$$\bar{T}_1 = [3\tilde{q}_1 + 2\tilde{q}_2]^2\bar{\eta}_1 + 2\tilde{q}_1\eta_2[3\tilde{q}_1 + 4\tilde{q}_2] \tag{32}$$

$$\bar{T}_2 = 4[\tilde{q}_2]^2\bar{\eta}_2 \tag{33}$$

The ensemble-volume averaged 'current stress norm' for any point $\mathbf{x}$ in three-dimensional random fiber composites can be defined as

$$\sqrt{\langle H\rangle(\mathbf{x})} = (1 - \phi_1 - \phi_2)\sqrt{\subset \bar{\boldsymbol{\sigma}} \supset : \subset \bar{\mathbf{T}} \supset : \subset \bar{\boldsymbol{\sigma}} \supset} \tag{34}$$

where ϕ_1 and ϕ_2 are volume fractions of the current perfectly bonded fibers and penny-shaped microcracks, respectively. Therefore, the effective yield function for the four-phase, three-dimensional random fiber composites can be proposed as

$$\bar{F} = (1 - \phi_1 - \phi_2)^2 \subset \bar{\boldsymbol{\sigma}} \supset : \subset \bar{\mathbf{T}} \supset : \subset \bar{\boldsymbol{\sigma}} \supset - K^2(\bar{e}^p) \tag{35}$$

with the isotropic hardening function $K(e^p)$ for the four-phase composite. The effective ensemble-volume averaged

plastic strain rate for the three-dimensional random fiber composites can be expressed as

$$\dot{\bar{\boldsymbol{\epsilon}}}^p = \dot{\lambda}\frac{\partial \bar{F}}{\partial \bar{\boldsymbol{\sigma}}} = 2(1-\phi_1-\phi_2)^2\dot{\lambda} \subset \bar{\mathbf{T}} \supset : \subset \bar{\boldsymbol{\sigma}} \supset \tag{36}$$

where $\dot{\lambda}$ signifies the plastic consistency parameter.

The effective equivalent plastic strain rate for the composite is defined as

$$\dot{\bar{e}}^p \equiv \sqrt{\frac{2}{3}\dot{\bar{\boldsymbol{\epsilon}}}^p \subset \bar{\mathbf{T}} \supset^{-1} : \dot{\bar{\boldsymbol{\epsilon}}}^p}$$

$$= 2(1-\phi_1-\phi_2)^2\dot{\lambda}\sqrt{\frac{2}{3} \subset \bar{\boldsymbol{\sigma}} \supset : \subset \bar{\mathbf{T}} \supset : \subset \bar{\boldsymbol{\sigma}} \supset} \tag{37}$$

The $\dot{\lambda}$ together with the yield function $\bar{F}$ must obey the Kuhn–Tucker loading/unloading conditions. The simple power-law type isotropic hardening function is employed as an example:

$$K(\bar{e}^p) = \sqrt{\frac{2}{3}}\{\sigma_y + h(\bar{e}^p)^{\bar{q}}\} \tag{38}$$

where σ_y is the initial yield stress, and h and $\bar{q}$ signify the linear and exponential isotropic hardening parameters (respectively) for the four-phase composite.

2.3. Progressive fiber debonding

The evolutionary interfacial debonding occurs under increasing loads or deformations and influences the overall behavior of crack-weakened, chopped fiber composites. After the interfacial debonding, the debonded fibers lose the load-carrying capacity along the debonded direction and are regarded as partially debonded fibers. Following Zhao and Weng [7,8] and Ju and Lee [9], the probability of partial debonding is modeled as a two-parameter Weibull process. Assuming that the Weibull statistics govern, the cumulative probability distribution function of fiber debonding (damage) P_d at the level of hydrostatic tensile stress $(\bar{\boldsymbol{\sigma}}_m)_1$ can be expressed as

$$P_d[(\bar{\boldsymbol{\sigma}}_m)_1] = 1 - \exp\left[-\left(\frac{(\bar{\sigma}_m)_1}{S_o}\right)^M\right] \tag{39}$$

with $(\bar{\boldsymbol{\sigma}}_m)_1 = (1-(2/3)\nu_1)(\bar{\sigma}_{kk})_1$, where ν_1 denotes the Poissson's ratio of the fibers and $(\bar{\sigma}_{kk})_1$ is the average hydrostatic tensile stress of the fibers. Constants S_o and M are the Weibull parameters.

Therefore, the current partially debonded (damaged) fiber volume fraction ϕ_2 at a given level of $(\bar{\boldsymbol{\sigma}}_m)_1$ is given by

$$\phi_2 = \phi P_d[((\bar{\boldsymbol{\sigma}}_m)_1 = \phi\left\{1 - \exp\left[-\left(\frac{(\bar{\boldsymbol{\sigma}}_m)_1}{S_o}\right)^M\right]\right\} \tag{40}$$

where ϕ is the original fiber volume fraction.

The formulation for the internal stresses of fibers needed to initiate interfacial debonding can be found in Lee and Simunovic [13]; see Eqs. (75)–(89) therein.

3. Finite element implementation

To describe the various phenomena taking place during impact, it is necessary to characterize the behavior of materials under impact loading conditions. The characterization involves not only the stress–strain response at large strains and different strain rates, but also the accumulation of damage and the mode of failure. Such complex material damage behavior under dynamic loading is difficult to describe in analytical models. In numerical simulations, constitutive models of nearly any degree of complexity can be incorporated into the code. Therefore, the constitutive models derived are implemented into the nonlinear finite element code using a user-defined material subroutine to simulate the dynamic in-elastic behavior and the progressive damage of the composite materials. While the implicit integration is chosen with an automatic time increment because it is not restricted to mildly nonlinear deformations or short response times, the explicit method is computationally attractive when the response time of interest is within an order of magnitude of the time it takes for a stress wave to travel through the shell thickness. Accordingly, the developed damage models are implemented into the explicit finite element code DYNA3D for impact simulations that require a very small time step.

The methodology used in this work is based on the well-known strain-driven algorithm in which the stress history is to be uniquely determined by the given strain history, mainly because of its computational efficiency in the framework of the explicit time integration computer program DYNA3D. The two-step operator splitting methodology is also adopted here to split the elastoplastic loading process into the elastic predictor and the plastic corrector. More detailed information for strain driven algorithms, micromechanical iterative algorithms for the progressive damage models, and three-dimensional return mapping algorithms can be found in our previous research [14]. The implemented model is applicable for shell and solid elements in three-dimensional analysis, as well as axisymmetric elements in two-dimensional analysis. The main advantage of this model compared with most computational damage models is that the damage evolution, giving material degradation, is fully coupled with the constitutive equation by incorporating probabilistic micromechanics appropriate to the constitutive models.

4. Numerical examples

4.1. Effects of microcracks on the stress–strain behavior of composites

In the first numerical example, the proposed damage model is exercised numerically for a chopped glass fiber

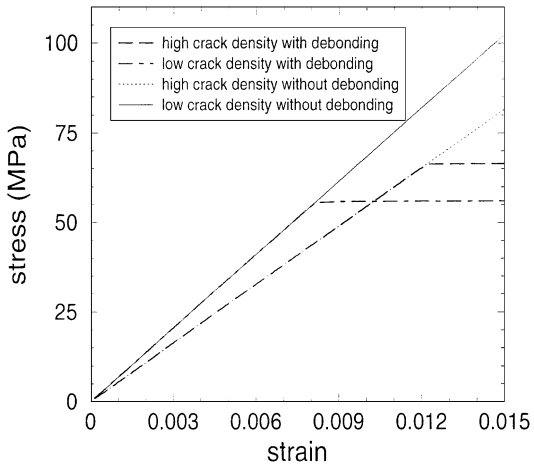

Fig. 1. Effects of microcracks on the stress–strain behavior of composites.

epoxy resin composite to investigate the effects of microcracks in the matrix on the stress–strain behavior composites. The material properties, aspect ratio of fibers, and Weibull parameters involving this simulation are: $E_0 = 3$ GPa, $\nu_0 = 0.35$, $E_1 = 72$ GPa, $\nu_1 = 0.17$, $\sigma_y = 125$ MPa, $h = 400$ MPa, $\bar{q} = 0.5$, $\alpha = 5$, $S_0 = 3406$ MPa, and $M = 250$. Fig. 1 exhibits the predicted stress–strain responses of crack-weakened composites with various crack densities and shows that the composite with low microcrack density is stiffer. It is noted from the numerical simulation that the stress–strain behavior of the composites is strongly dependent upon the microcrack density of the composites.

4.2. The cantilever beam test

The damage constitutive behavior of a cantilever beam is examined in numerical experiment. In the computation, the beam is fully clamped at the support and is subjected to a

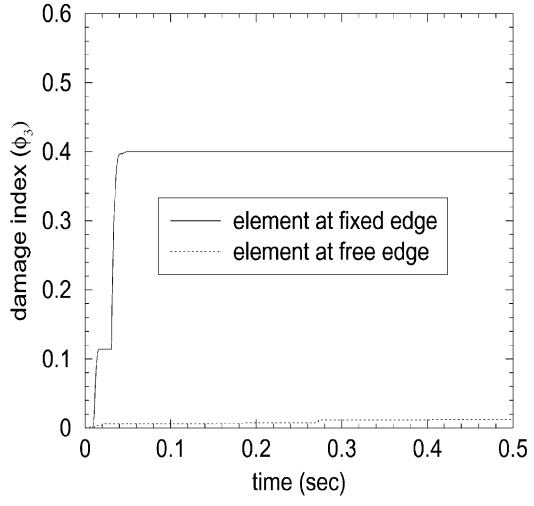

Fig. 2. Damage index of elements at free and fixed edges during impact.

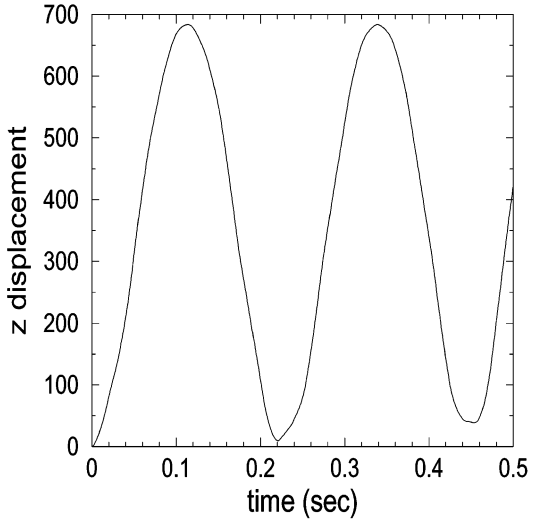

Fig. 3. Displacement in the z-direction at the free edge during impact.

force of 100 N in the z-direction at the free edge. The beam is 1000 mm in length; 100 mm in width; and 10 mm in thickness and is modeled by 10 Belytschko–Tsay shell elements. The calculation ends at 0.5 s. We employ the same material parameters for the composite beam as those used in Section 4.1. Here, the Weibull parameters for interfacial debonding and the initial volume fraction of fibers are chosen to be: $S_o = 3125$ MPa, $M = 4$, and $\phi_1 = 0.3$.

We exhibit the time-history plots for the damage index representing the volume fraction of damaged fibers during impact in Fig. 2. One may observe that the damage evolution at fixed edge is much quicker than that at free edge. Fig. 3 shows the displacement in the z-direction at the free edge indicating vibration relative to the equilibrium position under impact, which corresponds with the published results of LS-DYNA finite element simulations [15]. The simulation can be used for the identification of model characteristics for solving the boundary value problems.

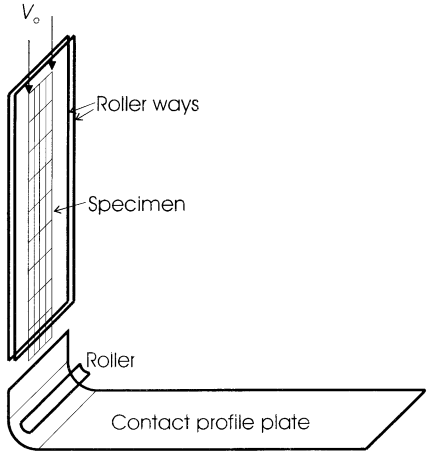

Fig. 4. Model problem: the composite contact test.

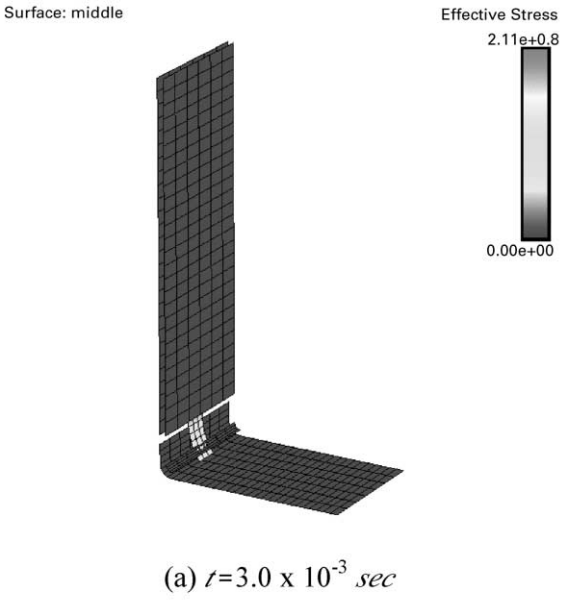

Fig. 5. von-Mises effective stress and deformation sequence of the composite plate.

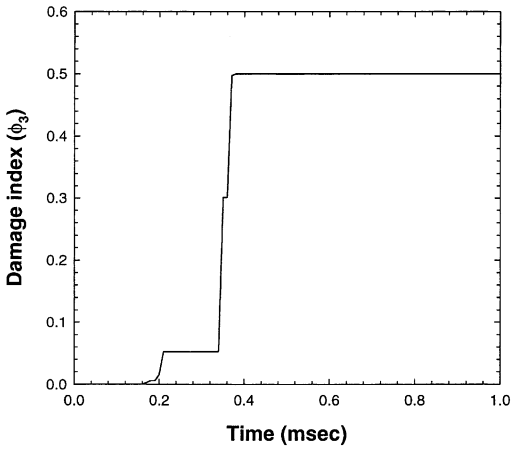

Fig. 6. A time history plot of the damage index at the top of the composite specimen.

4.3. The composite contact test

The experimental studies to characterize basic damage mechanisms and crashworthiness of chopped fiber composites have until now been limited in the literature. One such preliminary experimental study on chopped fiber composites was made by Starbuck et al. [16,17]. They developed an experimental set up for composite contact test and will conduct the test to investigate the dominant damage mechanisms that occurs during the progressive crushing of chopped carbon fiber composites.

Preliminary numerical simulations for the composite contact test are carried out to quantify the energy absorption and predict the damage evolution in the composites during the progressive crushing. In the computational model of the composite contact test as shown in Fig. 4, roller ways are modeled to reduce the unsupported length of specimen thereby preventing the specimen from buckling or folding and the roller at the bottom of the contact profile plate is used to provide a method of constraining the specimen to deform along the path of the constraint profile. In DYNA3D program, we specify roller ways, contact profile plate, and roller as the master rigid surface and the set of nodes on the composite specimen as the slave contact node set. The nodes at the top of the composite specimen are given at an initial velocity of 10 m/s in the negative direction. The default DYNA3D shell element formulation based on Belyschko–Tsay theory is utilized for modeling the composite specimen. We employ the same elastic properties, volume fraction and aspect ratio of fibers according to Starbuck et al. [17] as follows: $E_0 = 3$ GPa, $\nu_0 = 0.35$, $E_1 = 1000$ GPa, $\nu_1 = 0.17$, $\phi_1 = 0.3$, $\alpha = 5$. Since the plastic parameters σ_y, h and $\bar{q}$ were not reported in Starbuck et al. [16], we choose the plastic and Weibull parameters to be: $\sigma_y = 125$ MPa, $h = 400$ MPa, $\bar{q} = 0.5$, $S_o = 3406$ MPa, and $M = 250$.

From a sequence of intermediate numerical results displayed in Fig. 5, one can observe apparently specimen buckling between the contact plate profile and the roller. The roller ways are successful in preventing out-of-plane buckling in the carbon fiber composite specimen. A time history of the predicted damage index at the top of the specimen is plotted in Fig. 6. Fig. 7 shows a load–displacement trace at a node with prescribed velocity. The area under the load–displacement curve in Fig. 7 is the total energy absorption of the composite specimen. Further numerical simulations for the composite contact test with different profile radius, material property variables, and constraint

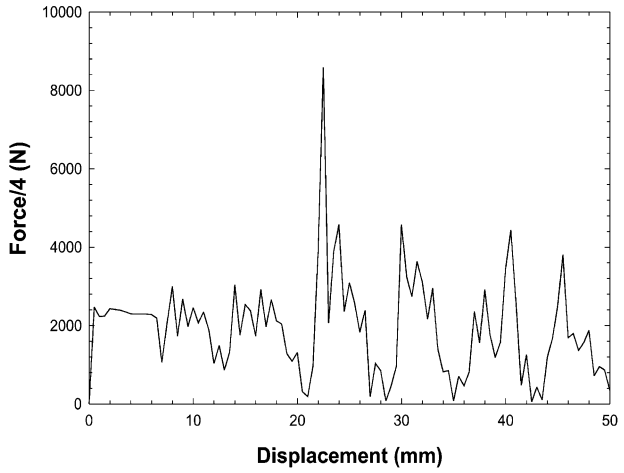

Fig. 7. A load–displacement trace at a node with prescribed velocity.

condition will be performed to meet the test conditions and compare with the test results that will be provided by Starbuck et al. [17].

5. Concluding remarks

A damage mechanics model of chopped fiber composites has been developed for predicting the damage constitutive behavior of the composites. Based on the statistically and micromechanically derived local stress norm, an effective yield criterion with isotropic hardening is constructed. The Weibull's probabilistic function is used to model the varying probability of progressive partial fiber debonding. The model is further extended to accommodate the effect of microcracks in the matrix. Finally, for practical applications of the proposed damage model on solving boundary value problems of composite materials under impact loading, the model is implemented into the finite element code DYNA3D. Numerical experiments for cantilever beam test and composite contact test are performed to assess the capability of the implemented model.

The model will be extended to accommodate the necessary failure mechanisms under impact. Moreover, further assessment and experimental model validation such as nondestructive testing for the proposed damage mechanics model will be conducted to solve crush problems encountered in practical engineering applications.

Acknowledgements

This research was sponsored by the US Department of Energy, Assistant Secretary for Energy Efficiency and Renewable Energy, Office of Transportation Technologies, Lightweight Materials Program, under contract DE-AC05-00OR22725 (Program Manager: Dr Joe Carpenter) with UT-Battelle, LLC.

Appendix A. Parameters Φ_{ij} and Ψ_i in Eq. (11)

These parameters are given by

$$\begin{aligned}\Phi_{ij} = &-\frac{1}{3} + \sum_{r=1}^{3} \frac{2\phi_r}{4725(1-\nu_0)^2(\mathscr{V}_r)_i(\mathscr{V}_r)_j} \\ &\times\Big\{1575(1-2\nu_0)^2(\mathscr{W}_r)_{ii}(\mathscr{W}_r)_{jj} \\ &+21(25\nu_0-23)(1-2\nu_0)[(\mathscr{W}_r)_{ii}(\mathscr{U}_r)_j + (\mathscr{W}_r)_{jj}(\mathscr{U}_r)_i] \\ &+21(25\nu_0-2)(1-2\nu_0)[(\mathscr{W}_r)_{ii}(\mathscr{W}_r)_{jj}] \\ &+3\Big(35\nu_0^2-70\nu_0+36\Big)(\bar{\mathscr{U}}_r)_{ij} + 7\Big(50\nu_0^2-59\nu_0+8\Big) \\ &\times[(\mathscr{U}_r)_i + (\mathscr{U}_r)_j] - 2\Big(175\nu_0^2-343\nu_0+103\Big)\Big\} \\ &(i,j=1,2)\end{aligned} \tag{A1}$$

$$\begin{aligned}\psi_i = &\frac{1}{2} + \sum_{r=1}^{3} \frac{\phi_r}{1575(1-\nu_0)(\mathscr{V}_r)_i(\mathscr{V}_r)_i} \\ &\times\Big\{\Big(72-140\nu_0+70\nu_0^2\Big)(Q_r)_i \\ &-\Big(75-266\nu_0+175\nu_0^2\Big)\frac{(\mathscr{R}_r)_i}{2} \\ &+\Big(164-476\nu_0+350\nu_0^2\Big)\Big\} \qquad (i=1,2,3)\end{aligned} \tag{A2}$$

where

$$(\mathscr{Q}_r)_1 = b_r, \qquad (\mathscr{Q}_r)_2 = d_r, \qquad (\mathscr{Q}_r)_3 = c_r \tag{A3}$$

$$\begin{aligned}&(\mathscr{R}_r)_1 = (\mathscr{Q}_r)_1 + (\mathscr{Q}_r)_2, \qquad (\mathscr{R}_r)_2 = 2(\mathscr{Q}_r)_2, \\ &(\mathscr{R}_r)_3 = (\mathscr{Q}_r)_1 + (\mathscr{Q}_r)_2\end{aligned} \tag{A4}$$

$$(\mathscr{V}_r)_i = 2[(\mathscr{Y}_r + \mathscr{B}_r)_i] \qquad (i=1,2,3) \tag{A5}$$

$$(\mathscr{W}_r)_{i1} = \frac{(Z_r)_{i1}}{J_r} \qquad (i=1,2,3) \tag{A6}$$

$$(\mathscr{W}_r)_{i2} = (\mathscr{W}_r)_{i3} = \frac{(Z_r)_{i2}}{J_r} \qquad (i=1,2,3) \tag{A7}$$

in which

$$\begin{aligned}(Z_r)_{i1} = &[2\mathscr{X}_r + 2(\mathscr{A}_r)_2 + (\mathscr{V}_r)_2][\mathscr{X}_r + (\bar{\mathscr{A}}_r)_{i1}] \\ &- 2[\mathscr{X}_r + (\mathscr{A}_r)_3][\mathscr{X}_r + (\bar{\mathscr{A}}_r)_{i2}] \\ &(i=1,2,3)\end{aligned} \tag{A8}$$

$$\begin{aligned}J_r = &[2\mathscr{X}_r + 2(\mathscr{A}_r)_2 + (\mathscr{V}_r)_2][\mathscr{X}_r + (\mathscr{A}_r)_1 + (\mathscr{V}_r)_1] \\ &- 2[\mathscr{X}_r + (\mathscr{A}_r)_3][\mathscr{X}_r + (\mathscr{A}_r)_4]\end{aligned} \tag{A9}$$

$$(Z_r)_{i2} = [2\mathscr{X}_r + (\mathscr{A}_r)_1 + (\mathscr{V}_r)_1][\mathscr{X}_r + (\bar{\mathscr{A}}_r)_{i2}] - [\mathscr{X}_r + (\mathscr{A}_r)_3][\mathscr{X}_r + (\bar{\mathscr{A}}_r)_{i1}] \quad (i = 1,2,3) \tag{A10}$$

and

$$(\mathscr{A}_r)_1 = (\bar{\mathscr{A}}_r)_{11}, \qquad (\mathscr{A}_r)_2 = (\bar{\mathscr{A}}_r)_{22},$$
$$(\mathscr{A}_r)_3 = (\bar{\mathscr{A}}_r)_{12}, \qquad (\mathscr{A}_r)_4 = (\bar{\mathscr{A}}_r)_{21}, \tag{A11}$$

$$(\mathscr{B}_r)_1 = (\bar{\mathscr{B}}_r)_{11}, \qquad (\mathscr{B}_r)_2 = (\bar{\mathscr{B}}_r)_{22}, \qquad (\mathscr{B}_r)_3 = (\bar{\mathscr{B}}_r)_{12} \tag{A12}$$

$$\mathscr{X}_r = \frac{\lambda_0\vartheta_r - \xi_r\mu_0}{(\vartheta_r - \mu_0)[2(\vartheta_r - \mu_0) + 3(\xi_r - \lambda_0)]} \tag{A13}$$

$$\mathscr{Y}_r = \frac{\mu_0}{2(\vartheta_r - \mu_0)} \tag{A14}$$

with

$$\xi_1 = \lambda_1, \qquad \vartheta_1 = \mu_1$$

$$\xi_2 = \frac{9\mu_1\kappa_1}{3\kappa_1 + 4\mu_1} - \mu_1, \qquad \vartheta_2 = \mu_1$$

$$\xi_3 = 0, \qquad \vartheta_3 = 0 \tag{A15}$$

where the parameters $(\bar{\mathscr{A}}_r)_{ij}$ and $(\bar{\mathscr{B}}_r)_{ij}$ read

$$(\bar{\mathscr{A}}_r)_{11} = \left(4\nu_0 + \frac{2}{\alpha_r^2 - 1}\right)\varpi_r + 4\nu_0 + \frac{4}{3(\alpha_r^2 - 1)} \tag{A16}$$

$$(\bar{\mathscr{A}}_r)_{12} = (\bar{\mathscr{A}}_r)_{13} = (S_r)_4 + (S_r)_5 \tag{A17}$$

$$(\bar{\mathscr{A}}_r)_{21} = (\bar{\mathscr{A}}_r)_{31} = (S_r)_3 + (S_r)_5 \tag{A18}$$

$$(\bar{\mathscr{A}}_r)_{22} = (\bar{\mathscr{A}}_r)_{23} = (\bar{\mathscr{A}}_r)_{32} = (\bar{\mathscr{A}}_r)_{33} = (S_r)_5 \tag{A19}$$

$$(\bar{\mathscr{B}}_r)_{11}\left(-4\nu_0 + \frac{4\alpha_r^2 - 2}{\alpha_r^2 - 1}\right)\varpi_r - 4\nu_0 + \frac{12\alpha_r^2 - 8}{3(\alpha_r^2 - 1)} \tag{A20}$$

$$(\bar{\mathscr{B}}_r)_{12} = (\bar{\mathscr{B}}_r)_{21} = (\bar{\mathscr{B}}_r)_{13} = (\bar{\mathscr{B}}_r)_{31} = (S_r)_2 + (S_r)_6 \tag{A21}$$

$$(\bar{\mathscr{B}}_r)_{22} = (\bar{\mathscr{B}}_r)_{33} = (\bar{\mathscr{B}}_r)_{23} = (\bar{\mathscr{B}}_r)_{32} = (S_r)_6 \tag{A22}$$

in which ν_0 denotes the Poisson's ratio of the matrix, and the components of Eshelby's tensor $(S_r)_1, \ldots, (S_r)_6$ and ϖ_r can be found in Lee and Simunovic [13].

In addition, the components of $(\mathscr{U}_r)_i$ and $(\bar{\mathscr{U}}_r)_{ij}$ in Eq. (A1) read

$$(\mathscr{U}_r)_1 = \frac{3\left[1 - \alpha_r^4 f\left(\alpha_r^2\right)\right]}{1 - 4\alpha_r^4} \tag{A23}$$

$$(\mathscr{U}_r)_2 = (\mathscr{U}_r)_3 = \frac{1}{2}[3 - (\mathscr{U}_r)_1] \tag{A24}$$

$$(\bar{\mathscr{U}}_r)_{ij} = \begin{bmatrix} b_r & c_r & c_r \\ c_r & d_r & d_r \\ c_r & d_r & d_r \end{bmatrix} \qquad (i,j = 1,2,3) \tag{A25}$$

with

$$f(\alpha_r) = \begin{cases} \dfrac{\cos^{-1}\alpha_r}{\alpha_r\sqrt{1 - \alpha_r^2}}, & \alpha_r < 1 \\ \dfrac{\cosh^{-1}\alpha_r}{\alpha_r\sqrt{\alpha_r^2 - 1}}, & \alpha_r > 1 \end{cases} \tag{A26}$$

and

$$b_r = \frac{5}{2(1 - \alpha_r^4)^2}\left[2 + \alpha_r^4 - 3\alpha_r^4 f\left(\alpha_r^2\right)\right] \tag{A27}$$

$$c_r = \frac{15\alpha_r^4}{4(1 - \alpha_r^4)^2}\left[-3 + \left(1 + 2\alpha_r^4\right)f\left(\alpha_r^2\right)\right] \tag{A28}$$

$$d_r = \frac{1}{8}(15 - 3b_r - 4c_r) \tag{A29}$$

References

[1] Lee HK, Simunovic S. Modeling of progressive damage in aligned and randomly oriented discontinuous fiber polymer matrix composites. Compos Part B: Engng 2000;31:77–86.

[2] Matzenmiller A, Schweizerhof K. Crashworthiness simulations of composite structures—a first step with explicit time integration. Munchen: CAD-FEM, 1991.

[3] Murray YD. Theory and verification of the fiber composite damage model implemented in DYNA3D. Tech Rep APTEC, 1989.

[4] Simunovic S, Zarcharia T. Application of high performance computing to automotive design and manufacturing. ORNL Tech Rep ORNL/TM-13444, 1997.

[5] Kutlu Z, Chang FK. Composite panels containing multiple through-the-width delaminations and subjected to compression. Part I: analysis. Compos Struct 1995;31:273–96.

[6] Meraghni F, Benzeggagh ML. Micromechanical modeling of matrix degradation in randomly discontinuous-fibre composites. Compos Sci Technol 1995;55:171–86.

[7] Zhao YH, Weng GJ. Plasticity of a two-phase composite with partially debonded inclusions. Int J Plasticity 1996;12:781–804.

[8] Zhao YH, Weng GJ. Transversely isotropic moduli of two partially debonded composites. Int J Solids Struct 1997;34:493–507.

[9] Ju JW, Lee HK. A micromechanical damage model for effective elastoplastic behavior of ductile matrix composites considering evolutionary complete particle debonding. J Computer Meth Appl Mech Engng 2000;183:201–22.

[10] Ju JW, Chen TM. Micromechanics and effective moduli of elastic composites containing randomly dispersed ellipsoidal inhomogeneities. Acta Mech 1994;103:103–21.

[11] Lee HK. A computational approach to the investigation of impact damage evolution in discontinuously reinforced fiber composites. Comput Mech 2001;27:504–12.

[12] Ju JW, Chen TM. Effective elastic moduli of two-phase composites containing randomly dispersed spherical inhomogeneities. Acta Mech 1994;103:123–44.

[13] Lee HK, Simunovic S. A damage constitutive model of progressive debonding in aligned discontinuous fiber composites. Int J Solids Struct 2000;38:875–95.

[14] Lee HK, Simunovic S. A micromechanical constitutive model of progressive crushing in random carbon fiber polymer matrix composites. ORNL Tech Rep ORNL/TM-1999/158, 1999.
[15] Reid JD. LS-DYNA example manual. Livermore: LSTC, 1998. p. 97–104.
[16] Starbuck JM, Simunovic S, Jacob GC. Test methodologies for determining energy absorbing mechanisms of automotive composite material systems. SAE Tech Pap Ser 2000;2000-01-1526:1–6.
[17] Starbuck JM, Simunovic S, Jacob GC. Test of chopped carbon fiber reinforced composites. In preparation.